Diversity and Outage Performance in Space–Time Block Coded Ricean MIMO Channels

Rohit U. Nabar, *Member, IEEE*, Helmut Bölcskei, *Senior Member, IEEE*, and Arogyaswami J. Paulraj, *Fellow, IEEE*

***Abstract*—The goal of this paper is to assess the impact of real-world propagation conditions on the maximum achievable diversity performance of communication over Ricean multiple-input multiple-output (MIMO) channels. To this end, we examine a MIMO channel employing orthogonal space–time block codes (OSTBCs) and study the diversity behavior of the resulting effective single-input single-output (SISO) channel. The performance criteria employed are symbol error rate, outage capacity, and wideband spectral efficiency. For general propagation conditions, we establish key quantities that determine performance irrespective of the performance criterion used. Furthermore, we discuss the relation between the notion of diversity order related to the slope of the average error probability versus signal-to-noise ratio (SNR) curve and diversity order related to the slope of the outage probability versus SNR curve. For Ricean fading MIMO channels, we demonstrate the existence of an SNR-dependent critical rate R_{crit}, below which signaling with zero outage is possible and, hence, the fading channel behaves like an additive white Gaussian noise (AWGN) channel. For SISO channels, R_{crit} is always zero. In the MIMO case, R_{crit} is a simple function of the angle between the vectorized Ricean component of the channel and the subspace spanned by the vectorized Rayleigh fading component.**

***Index Terms*—Multiple-input multiple-output (MIMO), outage probability, Ricean fading, spatial diversity, space–time coding.**

I. Introduction

WIRELESS links are impaired by random fluctuations in signal level known as fading. Diversity provides the receiver with multiple (ideally independent) replicas of the transmitted signal and is therefore a powerful means to combat fading. Space–time codes [1]–[4] are capable of extracting spatial diversity gain in systems employing multiple antennas at the transmitter and receiver (multiple-input multiple-output (MIMO) systems) without requiring channel knowledge in the transmitter. Orthogonal space–time block codes (OSTBCs) [3], [4] are particularly attractive since they yield maximum spatial diversity gain and, at the same time, decouple the vector detection problem into scalar detection problems, thereby significantly reducing decoding complexity (at the expense of spatial transmission rate).

Manuscript received December 20, 2003; revised May 15, 2004 and June 23, 2004; accepted June 28, 2004. The editor coordinating the review of this paper and approving it for publication is H. Li.

R. U. Nabar is with the DSP Technology Group, Marvell Semiconductor, Inc., Sunnyvale, CA 94089 USA (e-mail: rnabar@marvell.com).

H. Bölcskei is with the Communication Technology Laboratory, Swiss Federal Institute of Technology (ETH) Zürich, Zürich CH-8092, Switzerland (e-mail: boelcskei@nari.ee.ethz.ch).

A. J. Paulraj is with the Information Systems Laboratory, Stanford University, Stanford, CA 94305 USA (e-mail: apaulraj@stanford.edu).

Digital Object Identifier 10.1109/TWC.2005.853835

The performance of any space–time coding scheme depends strongly on the MIMO channel statistics, which, in turn, depend on antenna characteristics, height and spacing, and scattering richness. The classical independent identically distributed (i.i.d.) Rayleigh frequency-flat fading MIMO channel model [2] assumes that the elements of the matrix channel are i.i.d. zero-mean circularly symmetric complex Gaussian distributed. Measurements reveal, however, that, in practice, the MIMO channel deviates significantly from this idealistic behavior [5]. In this paper, we consider a general MIMO channel model that allows Rayleigh or Ricean fading and arbitrary scalar channel gains and correlation between matrix elements.

A. Contributions

The goal of this paper is to assess the impact of real-world propagation conditions on maximum achievable diversity performance in MIMO channels. OSTBCs convert the MIMO channel into a single-input single-output (SISO) channel with the effective channel gain given by the square-root of the sum of the squared magnitudes of the complex-valued scalar subchannel gains [4]. All the degrees of freedom in the channel are utilized to realize diversity gain, and the multiplexing gain [6] equals 1. The ultimate diversity performance of a general MIMO channel can therefore be assessed by studying the performance limits of the effective SISO channel resulting from the application of OSTBCs. Commonly used performance measures in fading channels are outage capacity [7], average symbol error rate [8], and wideband spectral efficiency [9]. The detailed contributions reported in this paper can be summarized as follows.

1) We quantify analytically the impact of Ricean fading, spatial fading correlation, and channel gain imbalance on outage capacity, average symbol error rate, and wideband spectral efficiency and establish key quantities (as a function of the propagation parameters) determining performance, irrespective of the performance criterion used.
2) We exhibit and quantify the critical performance determining role played by the angle between the vectorized Ricean component and the range space of the fading correlation matrix pertaining to the Rayleigh component of the channel.
3) For Ricean channels, we demonstrate the existence of a critical rate, below which signaling with zero outage is possible, or, equivalently, the channel behaves like an additive white Gaussian noise (AWGN) channel. For fading SISO channels, this critical rate is always zero. In the

MIMO case, the critical rate is a simple function of the angle between the vectorized Ricean component and the range space of the correlation matrix corresponding to the Rayleigh component. Moreover, we show that for a fixed transmission rate, channels with nonzero critical rate have a diversity order of ∞, whereas in the case of the critical rate being equal to zero, the diversity order is given by the rank of the fading correlation matrix.

4) We demonstrate that the notions of diversity order related to the slope of the error probability versus signal-to-noise ratio (SNR) curve, and diversity order related to the slope of the outage probability versus SNR curve yield equivalent results.
5) Finally, we provide analytical expressions for outage probability (as a function of the propagation parameters), which lend themselves to efficient numerical evaluation.

B. Relation to Previous Work

We note that the effective channel for OSTBCs resembles the effective channel obtained for maximum ratio combining (MRC) [10], [11], the performance of which has been studied extensively [11]–[14]. Noting that Ricean fading is a special case of Nakagami fading, the results in [11]–[13] can be used to compute (numerically) the outage probability of OSTBCs under Ricean fading. In this paper, we provide alternative power and Laguerre series-based expressions for the outage probability of OSTBCs under Ricean fading. In particular, the power series expansion allows us to characterize the outage performance analytically.

Previously, the equivalence of diversity characterization through average and outage error rate performance for a broader class of fading channels (Nakagami-q, n, m distributions) with finite code books has been demonstrated in [14]. We show that the same equivalence result is obtained in Ricean channels through an average symbol error rate and outage probability [packet error rate (PER)] analysis assuming Gaussian code books in the latter case.

The performance of space–time codes under correlated Rayleigh fading and Ricean fading has been studied in [2] and [15]–[21]. The impact of propagation conditions on the wideband spectral efficiency of MIMO channels has been studied previously in [22]. Compared to [2] and [15]–[22], our analysis reveals the critical performance determining role of the angle between the vectorized Ricean component and the range space of the correlation matrix associated with the Rayleigh fading component. Moreover, our results establish the presence of a previously unknown critical transmission rate, below which a Ricean MIMO channel (in conjunction with an OSTBC) behaves like an AWGN channel, and above which it appears as Rayleigh fading.

C. Notation

The superscripts $^{\mathrm{T}}$, $^{\mathrm{H}}$, * stand for transposition, conjugate transposition, and elementwise conjugation, respectively. $\mathcal{E}$ denotes the expectation operator. $\mathbf{0}_{m,n}$ stands for the $m \times n$ all-zeros matrix. $\mathbf{I}_m$ is the $m \times m$ identity matrix. $\mathrm{Tr}(\mathbf{A})$, $\|\mathbf{A}\|_F = \sqrt{\mathrm{Tr}(\mathbf{A}\mathbf{A}^{\mathrm{H}})}$, $r(\mathbf{A})$, $\mathcal{R}(\mathbf{A})$, $\mathcal{N}(\mathbf{A})$, and $\mathbf{A}^{\dagger}$ denote the trace, Frobenius norm, rank, range space, null space, and pseudo-inverse, respectively, of the matrix $\mathbf{A}$. $\Re(\mathbf{A})$ and $\Im(\mathbf{A})$ stand for the real and imaginary parts of $\mathbf{A}$, respectively. $\|\mathbf{a}\|$ denotes the Euclidean norm of the vector $\mathbf{a}$. For an $m \times n$ matrix $\mathbf{A} = [\mathbf{a}_1\ \mathbf{a}_2\ \ldots\ \mathbf{a}_n]$, we define the $mn \times 1$ vector $\mathrm{vec}(\mathbf{A}) = [\mathbf{a}_1^{\mathrm{T}}\ \mathbf{a}_2^{\mathrm{T}}\ \ldots\ \mathbf{a}_n^{\mathrm{T}}]^{\mathrm{T}}$. $u(y)$ denotes the unit-step function defined as $u(y) = 1$ for $y \geq 0$ and 0 otherwise. A circularly symmetric complex Gaussian random variable is a random variable $Z = X + jY \sim \mathcal{CN}(0, \sigma^2)$, where X and Y are i.i.d. $\mathcal{N}(0, \sigma^2/2)$. Unless specified otherwise, all logarithms are to the base 2.

D. Organization of the Paper

The remainder of this paper is organized as follows. In Section II, we present the general MIMO channel model, the associated signal model, and a simplified channel model used in our simulation examples. In Section III, we discuss the different performance criteria analyzed in the paper. In Section IV, we provide the power series and Laguerre series expansions for the cumulative distribution function (cdf) of the squared Frobenius norm of the MIMO channel matrix. In Sections V, VI, and VII, we study the impact of propagation conditions on OSTBC average symbol error rate, outage capacity, and wideband spectral efficiency, respectively. We conclude in Section VIII.

II. MIMO Channel and Signal Model

In this section, we introduce the MIMO channel model used throughout this paper, followed by a brief description of the signal model for OSTBCs.

A. General MIMO Channel Model

We consider a frequency-flat fading MIMO channel with M_{T} transmit and M_{R} receive antennas. The corresponding $M_{\mathrm{R}} \times M_{\mathrm{T}}$ random channel matrix $\mathbf{H} = \overline{\mathbf{H}} + \widetilde{\mathbf{H}}$ is decomposed into the sum of a fixed [possibly line-of-sight (LOS)] component $\overline{\mathbf{H}} = \mathcal{E}\{\mathbf{H}\}$ and a variable (or scattered) component $\widetilde{\mathbf{H}}$. In the case of pure Rayleigh fading, $\overline{\mathbf{H}} = \mathbf{0}_{M_{\mathrm{R}},M_{\mathrm{T}}}$, whereas in the case of Ricean fading, $\overline{\mathbf{H}} \neq \mathbf{0}_{M_{\mathrm{R}},M_{\mathrm{T}}}$. Throughout the remainder of this paper, we let $N = M_{\mathrm{T}}M_{\mathrm{R}}$ and apply the channel power normalization $\mathcal{E}\{\|\mathbf{H}\|_F^2\} = \|\overline{\mathbf{H}}\|_F^2 + \mathcal{E}\{\|\widetilde{\mathbf{H}}\|_F^2\} \leq N$. Furthermore, we assume that the channel is block fading [23] so that $\mathbf{H}$ remains constant over $T \geq M_{\mathrm{T}}$ symbol periods and changes in an independent fashion from block to block. The elements of $\widetilde{\mathbf{H}}$ are circularly symmetric complex Gaussian random variables. With large antenna spacing, rich scattering in the propagation environment, and all antenna elements employing identical polarization, the scalar subchannels of $\widetilde{\mathbf{H}}$ can, furthermore, be assumed i.i.d. In practice, however, these conditions are hardly met so that the elements of $\widetilde{\mathbf{H}}$ will be correlated with possibly different variances resulting from power/gain imbalance and/or the use of different antenna polarizations. Defining $\widetilde{\mathbf{h}} = \mathrm{vec}(\widetilde{\mathbf{H}})$, the statistics of $\widetilde{\mathbf{H}}$ are characterized by the $N \times N$ correlation matrix $\mathbf{R} = \mathcal{E}\{\widetilde{\mathbf{h}}\widetilde{\mathbf{h}}^{\mathrm{H}}\}$ with eigendecomposition $\mathbf{R} = \mathbf{U}\mathbf{\Sigma}\mathbf{U}^{\mathrm{H}}$, where $\mathbf{\Sigma} = \mathrm{diag}\{\sigma_j\}_{j=1}^{N}$ with the ordering $\sigma_j \geq \sigma_{j+1} (j = 1, 2, \ldots, N-1)$. Furthermore, we set

$\mathbf{h} = \mathrm{vec}(\mathbf{H})$ and $\overline{\mathbf{h}} = \mathrm{vec}(\overline{\mathbf{H}})$. Note that $\overline{\mathbf{h}}$ and $\mathbf{R}$ completely characterize the statistics of the Ricean MIMO channel. We finally note that the classical i.i.d. Rayleigh fading MIMO channel is recovered for $\overline{\mathbf{h}} = \mathbf{0}_{N,1}$ and $\mathbf{R} = \mathbf{I}_N$.

B. Signal Model

The input–output relation is given by

$$\mathbf{y} = \sqrt{\frac{E_s}{M_{\mathrm{T}}}}\mathbf{H}\mathbf{s} + \mathbf{n}$$

where $\mathbf{y}$ denotes the $M_{\mathrm{R}} \times 1$ received signal vector, E_s is the total average energy available at the transmitter over a symbol period, $\mathbf{s}$ is the $M_{\mathrm{T}} \times 1$ transmit signal vector, and $\mathbf{n}$ is $M_{\mathrm{R}} \times 1$ spatiotemporally white noise with $\mathcal{E}\{\mathbf{n}\mathbf{n}^{\mathrm{H}}\} = N_0\mathbf{I}_{M_{\mathrm{R}}}$. We impose the transmit power constraint $\mathrm{Tr}(\mathcal{E}\{\mathbf{s}\mathbf{s}^{\mathrm{H}}\}) = M_{\mathrm{T}}$. Throughout the paper, we assume that the channel matrix $\mathbf{H}$ is unknown at the transmitter and perfectly known at the receiver. Finally, we note that the use of OSTBCs combined with appropriate processing at the receiver [4] turns the matrix channel $\mathbf{H}$ into an effective SISO channel with input–output relation

$$y = \sqrt{\frac{E_s}{M_{\mathrm{T}}}}\|\mathbf{H}\|_F s + n \tag{1}$$

where y denotes the scalar processed received signal, s is the scalar transmitted signal, and n is $\mathcal{CN}(0, N_0)$ white noise. We note that the results in this paper are not restricted to OSTBCs but apply more generally to any scheme resulting in the signal model (1). Examples of such schemes include MRC in a single-input multiple-output (SIMO) channel or RAKE reception in a code division multiple access (CDMA) channel with intersymbol interference (ISI).

C. Simplified Channel Model for Simulation Examples

For the sake of simplicity, in the simulation examples presented in the remainder of the paper, we limit the number of variable channel parameters and consider a system with two transmit and one or two receive antennas. The fixed and variable channel components are given by

$$\overline{\mathbf{H}} = \sqrt{\frac{K}{1+K}}\begin{bmatrix}1 & 1\\ 1 & 1\end{bmatrix} \quad \widetilde{\mathbf{H}} = \sqrt{\frac{1}{1+K}}\begin{bmatrix}\widetilde{g}_{1,1} & \widetilde{g}_{1,2}\\ \widetilde{g}_{2,1} & \widetilde{g}_{2,2}\end{bmatrix} \tag{2}$$

where $K \geq 0$ denotes the Ricean K-factor [24]. Furthermore, we define the following correlation coefficients

$$t = \frac{\mathcal{E}\left\{\widetilde{g}_{1,1}\widetilde{g}_{1,2}^*\right\}}{\sqrt{\mathcal{E}\left\{|\widetilde{g}_{1,1}|^2\right\}\mathcal{E}\left\{|\widetilde{g}_{1,2}|^2\right\}}} = \frac{\mathcal{E}\left\{\widetilde{g}_{2,1}\widetilde{g}_{2,2}^*\right\}}{\sqrt{\mathcal{E}\left\{|\widetilde{g}_{2,1}|^2\right\}\mathcal{E}\left\{|\widetilde{g}_{2,2}|^2\right\}}}$$

$$r = \frac{\mathcal{E}\left\{\widetilde{g}_{1,1}\widetilde{g}_{2,1}^*\right\}}{\sqrt{\mathcal{E}\left\{|\widetilde{g}_{1,1}|^2\right\}\mathcal{E}\left\{|\widetilde{g}_{2,1}|^2\right\}}} = \frac{\mathcal{E}\left\{\widetilde{g}_{1,2}\widetilde{g}_{2,2}^*\right\}}{\sqrt{\mathcal{E}\left\{|\widetilde{g}_{1,2}|^2\right\}\mathcal{E}\left\{|\widetilde{g}_{2,2}|^2\right\}}}$$

where t and r will be referred to as the transmit and receive correlation coefficients, respectively. Measurements have shown [5] that the correlation between the diagonal elements $\widetilde{g}_{1,1}$ and $\widetilde{g}_{2,2}$, and the antidiagonal elements $\widetilde{g}_{1,2}$ and $\widetilde{g}_{2,1}$, is typically very small compared to t and r. In the simplified channel model, we shall therefore assume that $\mathcal{E}\{\widetilde{g}_{1,1}\widetilde{g}_{2,2}^*\} = \mathcal{E}\{\widetilde{g}_{1,2}\widetilde{g}_{2,1}^*\} = 0$. Note that the simplified correlation model is equivalent to the Kronecker correlation model in [16], [25], [26] if rt is small. Furthermore, unless specified otherwise, we set $\mathcal{E}\{|\widetilde{g}_{i,j}|^2\} = 1 (i, j = 1, 2)$. When simulating a channel with a single receive antenna, we consider the two-input one-output channel corresponding to only the first row of the matrix $\mathbf{H} = \overline{\mathbf{H}} + \widetilde{\mathbf{H}}$, with $\overline{\mathbf{H}}$ and $\widetilde{\mathbf{H}}$ as defined in (2).

We finally emphasize that the analytical results presented in this paper hold for the general MIMO channel model described in Section II-A. The simplified channel model introduced in this subsection will be employed in our simulation examples only.

III. Performance Criteria

The performance limits of communication over fading channels are often quantified through average symbol error rate, outage capacity, and wideband spectral efficiency. In the following, we briefly describe these criteria and introduce the definitions used subsequently.

A. Uncoded Average Symbol Error Rate

Assuming quadrature amplitude modulation (QAM), the probability of (uncoded) symbol error for a given channel realization $\mathbf{H}$ can be approximated by [27], [28]

$$P_e = \overline{N}_e Q\left(\sqrt{\frac{\rho d_{\min}^2}{2M_{\mathrm{T}}}\|\mathbf{H}\|_F^2}\right) \tag{3}$$

where $\rho = E_s/N_0$ denotes the SNR and $\overline{N}_e$ and $d_{\min}$ stand for the average number of nearest neighbors and the minimum distance of separation of the underlying constellation, respectively. Applying the Chernoff bound $Q(x) \leq \exp[-(x^2/2)]$ to (3), we get

$$P_e \leq \overline{N}_e \mathrm{e}^{-\frac{\rho d_{\min}^2\|\mathbf{H}\|_F^2}{4M_{\mathrm{T}}}}.$$

Consequently, the average (over the channel $\mathbf{H}$) uncoded symbol error rate $\overline{P}_e = \mathcal{E}\{P_e\}$ can be upper bounded as

$$\overline{P}_e \leq \overline{N}_e \psi(\eta\rho) \tag{4}$$

where $\eta = d_{\min}^2/(4M_{\mathrm{T}})$ is a constellation-specific constant and $\psi(s) = \mathcal{E}\{\exp(-s\|\mathbf{H}\|_F^2)\}$ is the moment-generating function (MGF) of $\|\mathbf{H}\|_F^2$. Traditionally, the diversity order offered by a fading channel is defined as the magnitude of the high-SNR slope of average error probability as a function of SNR (on a log–log scale) [8], [29]. Based on this concept, the maximum achievable diversity order over a general MIMO channel (i.e., the diversity order achieved by OSTBCs) is given by

$$d_{\mathrm{E}} = -\lim_{\rho\to\infty}\frac{\log\overline{P}_e}{\log\rho} \geq -\lim_{\rho\to\infty}\frac{\log\psi(\eta\rho)}{\log\rho}$$

where the subscript E in d_{E} relates to the average error probability. Since the Chernoff bound is tight for high SNR [29], we can take [2]

$$d_{\mathrm{E}} = -\lim_{\rho\to\infty} \frac{\log \psi(\eta\rho)}{\log \rho}. \tag{5}$$

B. Outage Capacity

By virtue of the scalar nature of the effective channel induced by OSTBCs [cf. (1)], assuming a scalar Gaussian code book, the corresponding mutual information is given by [30]

$$I = r_c \log\left(1 + \frac{\rho}{M_{\mathrm{T}}}\|\mathbf{H}\|_F^2\right) \text{ bps/Hz}$$

where $r_c \leq 1$ denotes the spatial rate of the space–time block code as defined in [4].

Since $\mathbf{H}$ is random, the mutual information I will be a random variable. The outage probability corresponding to transmission rate R is defined as $P_{\mathrm{out}}(R) = P(I \leq R)$ [7], [23]. Equivalently, one can characterize the outage behavior by specifying the $q\%$ outage capacity $C_{\mathrm{out}}(q\%)$ as the capacity that is guaranteed for $(100-q)\%$ of the channel realizations, i.e., $P(I \leq C_{\mathrm{out}}(q\%)) = q\%$. Outage capacity is relevant when the length of the transmitted (temporal) codeword is restricted to be less than or equal to the fading block length. We can see that calculating the outage probability or outage capacity requires knowledge of the cdf of the random variable I. Denoting the cdf of $\|\mathbf{H}\|_F^2$ as $F(y)$, we have

$$P_{\mathrm{out}}(R) = F\left(\frac{\left(2^{\frac{R}{r_c}} - 1\right) M_{\mathrm{T}}}{\rho}\right)$$

and[1]

$$C_{\mathrm{out}}(q\%) = r_c \log\left(\frac{\rho}{M_{\mathrm{T}}} F^{-1}(q\%) + 1\right).$$

For the case where codewords span only one fading block, the outage probability can be related to PER as follows. Suppose we fix a transmission rate R. Since the channel is drawn randomly according to a given fading distribution, there will always be a nonzero probability that the mutual information corresponding to a given channel realization falls below R (no matter how small R is). Assuming that the transmitted codeword (packet) is decoded successfully if R is less than the mutual information of the given channel realization and declaring a decoding error otherwise, the outage probability equals the PER. This leads to the notion of a rate-dependent diversity order as defined in [31]

$$d_{\mathrm{O}}(R) = -\lim_{\rho\to\infty} \frac{\log P_{\mathrm{out}}(R)}{\log \rho} \tag{6}$$

where the subscript O in $d_{\mathrm{O}}(R)$ indicates that this definition relates to outage probability. Clearly, the statistics of $\|\mathbf{H}\|_F^2$ (which, in turn, depend on the channel conditions) will have a significant influence on the PER and, hence, the (rate-dependent) diversity order.

We finally note that in contrast to d_{E}, the quantity $d_{\mathrm{O}}(R)$ explicitly reflects the dependence of achievable diversity order on transmission rate R. Moreover, $d_{\mathrm{O}}(R)$ is relevant for Gaussian code books, whereas d_{E} pertains to finite code books. Since both definitions are frequently used in the literature, we will study the impact of propagation conditions on diversity order through an analysis of both d_{E} and $d_{\mathrm{O}}(R)$ and discuss the relation between the two quantities.

C. Spectral Efficiency in the Wideband Regime

A third frequently used measure to describe the severity of random fluctuations in the fading channel relates to the spectral efficiency in the wideband regime [9]. Assuming that the fading process is ergodic and coding can be performed over an infinite number of independently fading blocks, the spectral efficiency achieved by OSTBCs is given by

$$C(\rho) = r_c\, \mathcal{E}\left\{\log\left(1 + \frac{\rho}{M_{\mathrm{T}}}\|\mathbf{H}\|_F^2\right)\right\} \text{ bps/Hz} \tag{7}$$

where the expectation is taken with respect to the random channel $\mathbf{H}$. It is important to note that the use of OSTBCs can result in a considerable loss in spectral efficiency (compared to the true MIMO capacity). However, OSTBCs will perform well 1) in the very low-SNR regime (i.e., $\rho \ll 1$) or 2) if [2] the random MIMO channel has rank 1 with probability 1 (such as the pin-hole channel [26]). Following [9], we define $E_b/N_0 = \rho/C(\rho)$ as the SNR per information bit and $(E_b/N_0)_{\min}$ as the minimum E_b/N_0 required to sustain error-free communication. It is shown in [9, Th. 1] that $(E_b/N_0)_{\min} = \ln 2/\dot{C}(0)$ where $\dot{C}(\cdot)$ denotes the derivative of $C(\rho)$ in nats/s/Hz. It now follows that $\dot{C}(0) = (r_c\mu)/M_{\mathrm{T}}$ with $\mu = \mathcal{E}\{\|\mathbf{H}\|_F^2\}$. Invoking the power constraint $\mu \leq N = M_{\mathrm{T}}M_{\mathrm{R}}$, we obtain $(E_b/N_0)_{\min} \geq \ln 2/(r_c M_{\mathrm{R}})$, which reflects the fact that adding receive antennas reduces $(E_b/N_0)_{\min}$ due to receive array gain [6]. Since the channel is unknown to the transmitter, no transmit array gain can be realized.

The quantity we are interested in is the slope of the spectral efficiency as a function of E_b/N_0 (in bits per second per hertz per 3 dB) at $(E_b/N_0)_{\min}$ (i.e., the wideband slope). Applying [9, Th. 9] to (7), this slope is obtained as

$$\mathcal{S} = \frac{2r_c}{\kappa} \tag{8}$$

where $\kappa = \mathcal{E}\{\|\mathbf{H}\|_F^4\}/(\mathcal{E}\{\|\mathbf{H}\|_F^2\})^2$ is the kurtosis of $\|\mathbf{H}\|_F$. Denoting the standard deviation of $\|\mathbf{H}\|_F^2$ by $\sigma = (\mathcal{E}\{\|\mathbf{H}\|_F^4\} - (\mathcal{E}\{\|\mathbf{H}\|_F^2\})^2)^{1/2}$ it is easily seen that

$$\kappa = \mathrm{AF} + 1 \tag{9}$$

where $\mathrm{AF} = (\sigma/\mu)^2$ denotes the amount of fading as defined in [11] and [32]. The amount of fading is a widely used measure for quantifying the severity of random fluctuations in fading channels.

[1] $F^{-1}(y)$ denotes the inverse function of $F(y)$.

[2] OSTBCs are, in fact, capacity optimal for rank-1 MIMO channels if $r_c = 1$.

We conclude this section by noting that kurtosis is a measure of the peakiness of a distribution (or, equivalently, the randomness of the underlying random variable). The minimum value of kurtosis is 1, which is achieved if and only if the random variable is deterministic. As a consequence of these observations, we have

$$\mathcal{S} \leq 2r_c$$

with the upper bound being achieved if and only if the channel is AWGN. The wideband slope (8) can therefore be interpreted as a measure of the deviation of the fading channel from an AWGN channel. We finally note that the wideband slope for the MIMO channel $\mathcal{S}_{\mathrm{MIMO}}$ is lower bounded by the corresponding wideband slope for OSTBCs with $r_c = 1$, i.e., $\mathcal{S}_{\mathrm{MIMO}} \geq 2/\kappa$, where κ is defined in (8).

IV. Derivation of the CDF of $\|\mathbf{H}\|_F^2$

In the previous section, we have seen that specification of the diversity performance through average uncoded symbol error rate or PER requires computation of the MGF $\psi(s)$ and the cdf $F(y)$ of $\|\mathbf{H}\|_F^2$, respectively. Modifying the approach described in [33] to apply to the complex-valued case, we derive a closed-form expression for $\psi(s)$ in the Appendix [cf. (22)], based on which, again suitably modifying the approach in [33], we then find a power series expansion [cf. (24)] and a Laguerre series expansion [cf. (25)] for $F(y)$. We hasten to add that the results presented in the Appendix follow from a simple generalization of the approach reported in [33]. We have therefore restricted our exposition to providing only the key steps in the derivations. We note that an alternative series expansion for $F(y)$ has been presented in [34]. The resulting expressions for $F(y)$ in [34] are, in general, complicated and amenable to analytical studies only in certain special cases [35].

The convergence properties of the power series expansion in the low-outage regime allow us to analytically characterize PER-based diversity performance with relative ease. As noted in [33], the Laguerre series expansion on the other hand shows better convergence over a wider range of y. Generally, we observed that for $y \leq 2$, the power series converges faster than the Laguerre series. In the remainder of this paper, we shall use the power series expansion of $F(y)$ for analytical studies of the impact of the propagation conditions on the outage probability (or, equivalently, PER) in the low-outage regime. The Laguerre series expansion has been provided to allow numerical computation of the PER over a wide range of outage rates. We finally note that the truncation analysis in [36] can readily be extended to the complex-valued case to derive bounds on the residual error associated with summing a finite number of terms in the power and Laguerre series expansions. Moreover, denoting the truncation error that results from using only the first term (corresponding to $k = 0$) in the power series expansion (24) as $E(y)$, it follows from [36, eq. (121)] that $E(y) \propto y^{(r(\mathbf{R})+1)}e^{y/c}$ (with c arbitrarily chosen to satisfy $0 < c < \sigma_{r(\mathbf{R})}$) and, hence,

$$\lim_{y \to 0} E(y) = 0. \tag{10}$$

A. Numerical Example 1

This example is designed to demonstrate the difference in the convergence behavior of the power series and Laguerre series expansions of $F(y)$. In the following, $F_E(y)$ and $F_A(y)$ denote the empirically (through Monte Carlo methods) obtained cdf and the analytical cdf [obtained from (24) or (25)] of $\|\mathbf{H}\|_F^2$, respectively. We define the mean square error (MSE) between $F_E(y)$ and $F_A(y)$ as $\mathrm{MSE} = (1/M)\sum_{i=1}^{M} |F_E(y_i) - F_A(y_i)|^2$ with M uniformly spaced data points $y_i (i = 1, 2, \ldots, M)$ in the interval under consideration. For $M = 1000$, Fig. 1 shows the MSE as a function of the number of terms summed in the power and Laguerre ($\beta = 1$) series expansions, respectively, of $F(y) (0 \leq y \leq 8)$ for a channel with $K = 2$, $r = 0.1$, and $t = 0.2$ (cf. simplified channel model described in Section II-C). It is clearly seen that for a given MSE, the Laguerre series expansion requires significantly fewer terms than the power series expansion. The error floors in Fig. 1 can be attributed to the fact that beyond a certain number of terms in the series expansion, the error in empirical estimation of $F(y)$ dominates.

We shall next demonstrate the superiority of the power series expansion over the Laguerre series expansion for small values of y. For the same channel as in Fig. 1, Fig. 2 shows the empirically obtained cdf (through Monte Carlo methods) of $\|\mathbf{H}\|_F^2$ along with the power series expansion (24) of $F(y)$, calculated using the first term in the series expansion, and the Laguerre series expansion (25) of $F(y)$, calculated using the first and the first ten terms, respectively. The figure clearly shows that for small y, using the first term in the power series expansion (24) yields an excellent approximation of $F(y)$.

V. Uncoded Average Symbol Error Rate Performance

In this section, combining (4) and the expression for the MGF of $\|\mathbf{H}\|_F^2$ derived in the Appendix, we shall quantify the impact of the propagation conditions on $\overline{P}_e$ as well as the related definition of diversity order d_{E} given in (5). We start by inserting (22) into (4) and taking the logarithm of both sides to obtain

$$\log \overline{P}_e \leq \log \overline{N}_e - \eta\rho\|\overline{\mathbf{H}}\|_F^2 + \sum_{j=1}^{r(\mathbf{R})} \frac{(\eta\rho|b_j|)^2}{1+\eta\rho\sigma_j} - \sum_{j=1}^{r(\mathbf{R})} \log(1+\eta\rho\sigma_j). \tag{11}$$

Using (5) and setting $\delta = \|\overline{\mathbf{H}}\|_F^2 - \sum_{j=1}^{r(\mathbf{R})}(|b_j|^2/\sigma_j)$, it now follows that

$$d_{\mathrm{E}} = \lim_{\rho \to \infty} \left(\frac{\eta\rho\delta}{\log \rho} \right) + r(\mathbf{R}) \tag{12}$$

which, upon application of L'Hopital's rule, yields

$$d_{\mathrm{E}} = \begin{cases} \infty, & \delta > 0 \\ r(\mathbf{R}), & \delta = 0. \end{cases} \tag{13}$$

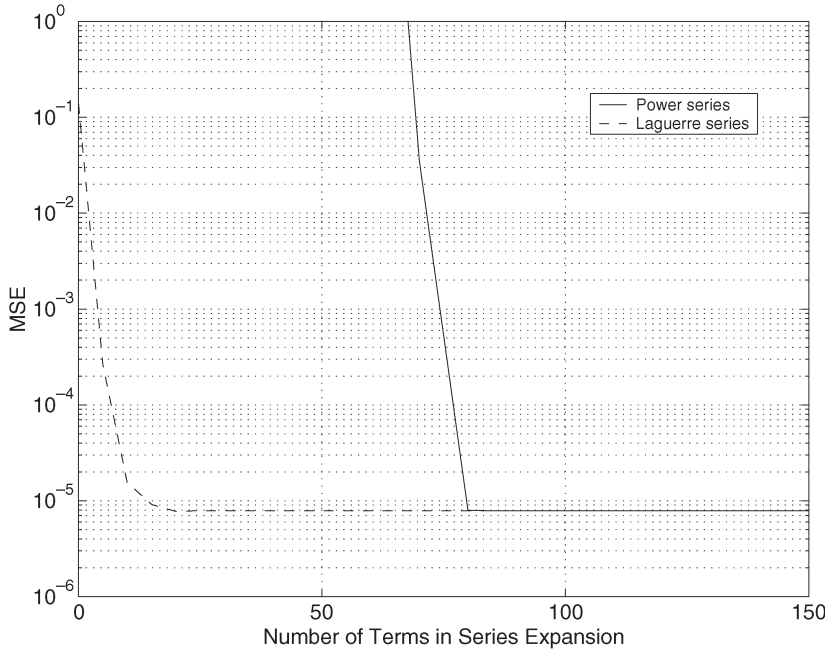

Fig. 1. Comparison of the convergence properties of the Laguerre series and the power series expansions of $F(y)$. The superior convergence property of the Laguerre series expansion is evident.

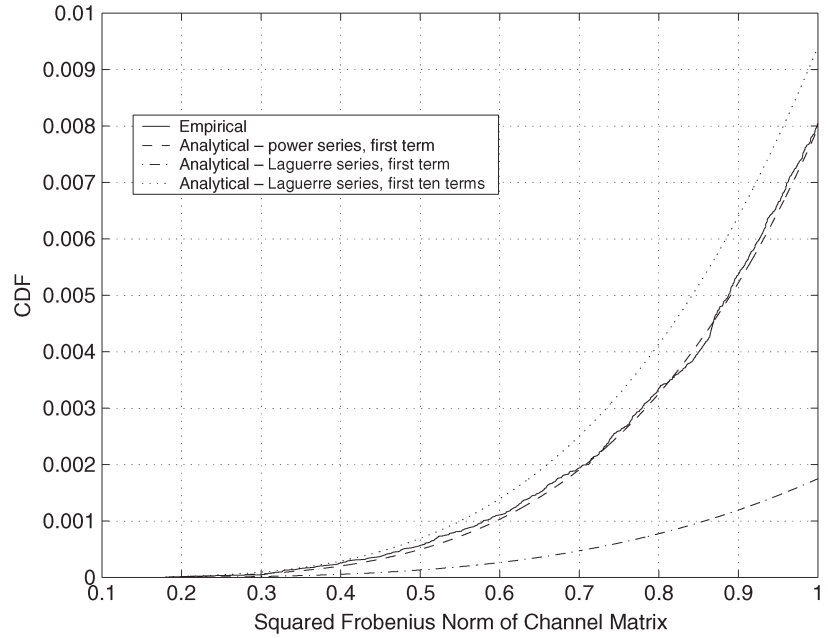

Fig. 2. Comparison of the approximation properties of the Laguerre series and the power series expansions of $F(y)$ for small y. The power series expansion exhibits superior numerical properties.

The case $\delta < 0$ is excluded since

$$\delta = \overline{\mathbf{h}}^{\mathrm{H}}\mathbf{U}\underbrace{\begin{bmatrix}\mathbf{0}_{r(\mathbf{R}),r(\mathbf{R})} & \mathbf{0}_{r(\mathbf{R}),N-r(\mathbf{R})}\\ \mathbf{0}_{N-r(\mathbf{R}),r(\mathbf{R})} & \mathbf{I}_{N-r(\mathbf{R})}\end{bmatrix}}_{\mathbf{A}}\mathbf{U}^{\mathrm{H}}\overline{\mathbf{h}} \geq 0. \quad (14)$$

Note that $\mathbf{UAU}^{\mathrm{H}} = \mathbf{I}_N - \mathbf{R}(\mathbf{R}^{\mathrm{H}}\mathbf{R})^{\dagger}\mathbf{R}^{\mathrm{H}}$, and, hence, δ may be interpreted as the squared Euclidean norm of the projection of $\overline{\mathbf{h}}$ onto $\mathcal{N}(\mathbf{R})$. Recalling that $\mathbf{U}$ contains the eigenvectors of $\mathbf{R}$, it follows that $\mathbf{UA}$ spans $\mathcal{N}(\mathbf{R})$, while $\mathbf{U}(\mathbf{I}_N - \mathbf{A})$ spans $\mathcal{R}(\mathbf{R})$. We can now conclude that equality in (14) is achieved in either of the following cases: 1) $\overline{\mathbf{h}} \neq \mathbf{0}_{N,1}$ and $r(\mathbf{R}) = N$; 2) $\overline{\mathbf{h}} = \mathbf{0}_{N,1}$ and $\mathbf{R}$ arbitrary; or 3) $\overline{\mathbf{h}} \neq \mathbf{0}_{N,1}$, $r(\mathbf{R}) < N$, and $\overline{\mathbf{h}}$ lies completely in $\mathcal{R}(\mathbf{R})$. This immediately implies that in the case of pure Rayleigh fading (i.e., $\overline{\mathbf{h}} = \mathbf{0}_{N,1}$), the diversity order is given by $d_{\mathrm{E}} = r(\mathbf{R})$. In the Ricean case, the situation is more complicated as both $d_{\mathrm{E}} = \infty$ and $d_{\mathrm{E}} = r(\mathbf{R})$ are possible. If the vector $\overline{\mathbf{h}}$ lies entirely in $\mathcal{R}(\mathbf{R})$, equality in (14) is achieved and $d_{\mathrm{E}} = r(\mathbf{R})$. If $\overline{\mathbf{h}}$ has nonzero components in $\mathcal{N}(\mathbf{R})$, we have $\delta > 0$ and, consequently, $d_{\mathrm{E}} = \infty$. This result has a nice physical interpretation: Let us start by investigating

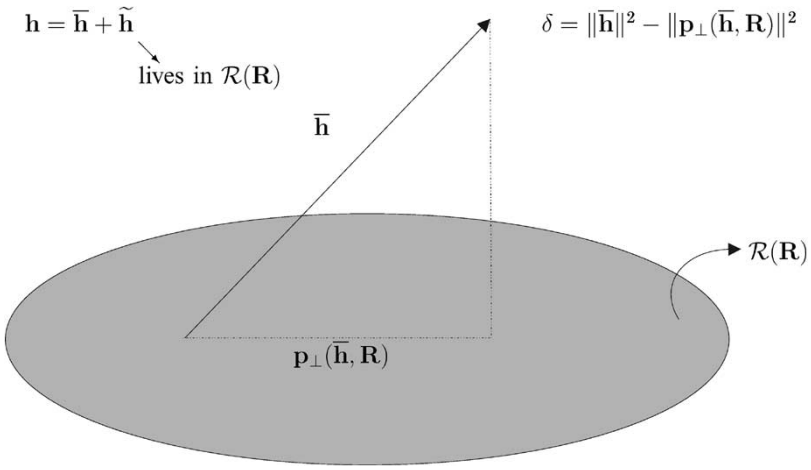

Fig. 3. Schematic illustrating the impact of the Hermitian angle between $\overline{\mathbf{h}}$ and $\mathcal{R}(\mathbf{R})$ on diversity order. If the Hermitian angle is nonzero, at least one of the $M_R M_T$ vectorized channel dimensions does not experience fading and the channel is effectively AWGN.

the SISO case where $h = \overline{h} + \widetilde{h}$ and (14) reduces to $\delta = \gamma|\overline{h}|^2$ with

$$\gamma = \begin{cases} 0, & K < \infty \\ 1, & K = \infty \end{cases}$$

where $K = |\overline{h}|^2/\mathcal{E}\{|\widetilde{h}|^2\}$ denotes the K-factor of the SISO channel. Employing (13), we can immediately conclude that $d_{\mathrm{E}} = 1$ for $K < \infty$ and $d_{\mathrm{E}} = \infty$ if $K = \infty$. Equivalently, this result says that the diversity order equals 1 as long as there is a Rayleigh fading component in the channel and the diversity order becomes ∞ for an AWGN channel.

We are now in a position to generalize this discussion to arbitrary MIMO channels with $N = M_{\mathrm{T}} M_{\mathrm{R}}$. The realizations of the N-dimensional vector $\mathbf{h} = \overline{\mathbf{h}} + \widetilde{\mathbf{h}}$ span a subspace that depends on $\overline{\mathbf{h}}$ and the subspace spanned by the realizations of $\widetilde{\mathbf{h}}$ and, hence, specified by $\mathbf{R}$. Now, in the case where $\overline{\mathbf{h}}$ lies entirely in the range space of $\mathbf{R}$ (and, hence, the subspace spanned by the realizations of $\widetilde{\mathbf{h}}$), all the dimensions "excited" by $\mathbf{h}$ will have a Rayleigh fading component so that, using our result above for the SISO case, the diversity order is simply the number of dimensions excited by $\mathbf{h}$, or, equivalently, $d_{\mathrm{E}} = r(\mathbf{R})$. In the case where the projection of $\overline{\mathbf{h}}$ onto $\mathcal{N}(\mathbf{R})$ is nonzero, we have at least one dimension that is purely AWGN, and, hence, by (13), we get $d_{\mathrm{E}} = \infty$. With the projection of $\overline{\mathbf{h}}$ onto $\mathcal{R}(\mathbf{R})$ given by

$$\mathbf{p}_\perp(\overline{\mathbf{h}}, \mathbf{R}) = \mathbf{R}(\mathbf{R}^{\mathrm{H}}\mathbf{R})^\dagger \mathbf{R}^{\mathrm{H}}\overline{\mathbf{h}}$$

we can rewrite

$$\delta = \|\overline{\mathbf{h}}\|^2 - \left\|\mathbf{p}_\perp(\overline{\mathbf{h}}, \mathbf{R})\right\|^2$$

and, hence, recover more formally that $d_{\mathrm{E}} = \infty$ whenever the projection of $\overline{\mathbf{h}}$ onto $\mathcal{N}(\mathbf{R})$ is nonzero. A more geometric interpretation is obtained by considering the Hermitian angle between $\overline{\mathbf{h}}$ and $\mathcal{R}(\mathbf{R})$ (see the equation at the bottom of the page) [37].

Note that $0 \le \angle(\overline{\mathbf{h}}, \mathcal{R}(\mathbf{R})) \le \pi/2$. We can now conclude that $0 < \angle(\overline{\mathbf{h}}, \mathcal{R}(\mathbf{R})) \le \pi/2$ implies a diversity order of ∞, whereas $\angle(\overline{\mathbf{h}}, \mathcal{R}(\mathbf{R})) = 0$ results in $d_{\mathrm{E}} = r(\mathbf{R})$. The situation is summarized in Fig. 3.

Besides the high-SNR slope of $\overline{P}_e$, the offset of the $\overline{P}_e$ curve will indicate the impact of the propagation conditions on uncoded average error rate performance. We shall therefore briefly discuss this aspect. Let us start with the high-SNR case (i.e., $\rho \gg 1$) where (11) simplifies to

$$\log \overline{P}_e \le \log \overline{N}_e - \eta\rho\delta - r(\mathbf{R}) \log(\eta\rho) - \sum_{j=1}^{r(\mathbf{R})} \log \sigma_j.$$

For fixed $\mathbf{R}$ with $r(\mathbf{R}) < N$, the upper bound on $\overline{P}_e$ is minimum if δ is maximum (i.e., the projection of $\overline{\mathbf{h}}$ onto $\mathcal{N}(\mathbf{R})$ is maximum) and all nonzero eigenvalues of $\mathbf{R}$ are equal. Hence, the Hermitian angle $\angle(\overline{\mathbf{h}}, \mathcal{R}(\mathbf{R}))$ has an important impact on the offset as well. For $r(\mathbf{R}) = N$ and, hence, $\angle(\overline{\mathbf{h}}, \mathcal{R}(\mathbf{R})) = 0$, the error rate performance is optimum if all the σ_j are equal, or, equivalently, $\mathbf{R} = \xi \mathbf{I}_N$ with $\xi = \mathcal{E}\{\|\widetilde{\mathbf{H}}\|_F^2\}/N$. In the low-SNR regime (i.e., $\rho \ll 1$), we have

$$\log \overline{P}_e \le \log \overline{N}_e - \eta\rho \left(\|\overline{\mathbf{H}}\|_F^2 + \mathrm{Tr}(\mathbf{R})\right) \tag{15}$$

which shows that the error rate performance is simply a function of the total power in the channel. Moreover, we can see that in the low-SNR regime, the geometry of $\overline{\mathbf{h}}$ relative to $\mathbf{R}$ as

$$\angle\left(\overline{\mathbf{h}}, \mathcal{R}(\mathbf{R})\right) = \begin{cases} 0, & \overline{\mathbf{h}} = \mathbf{0}_{N,1} \\ \cos^{-1}\left(\left|\frac{\overline{\mathbf{h}}^{\mathrm{H}}\mathbf{p}_\perp(\overline{\mathbf{h}},\mathbf{R})}{\|\overline{\mathbf{h}}\|\left\|\mathbf{p}_\perp(\overline{\mathbf{h}},\mathbf{R})\right\|}\right|\right), & \overline{\mathbf{h}} \neq \mathbf{0}_{N,1} \text{ and } \mathbf{p}_\perp(\overline{\mathbf{h}}, \mathbf{R}) \neq \mathbf{0}_{N,1} \\ \frac{\pi}{2}, & \overline{\mathbf{h}} \neq \mathbf{0}_{N,1} \text{ and } \mathbf{p}_\perp(\overline{\mathbf{h}}, \mathbf{R}) = \mathbf{0}_{N,1} \end{cases}$$

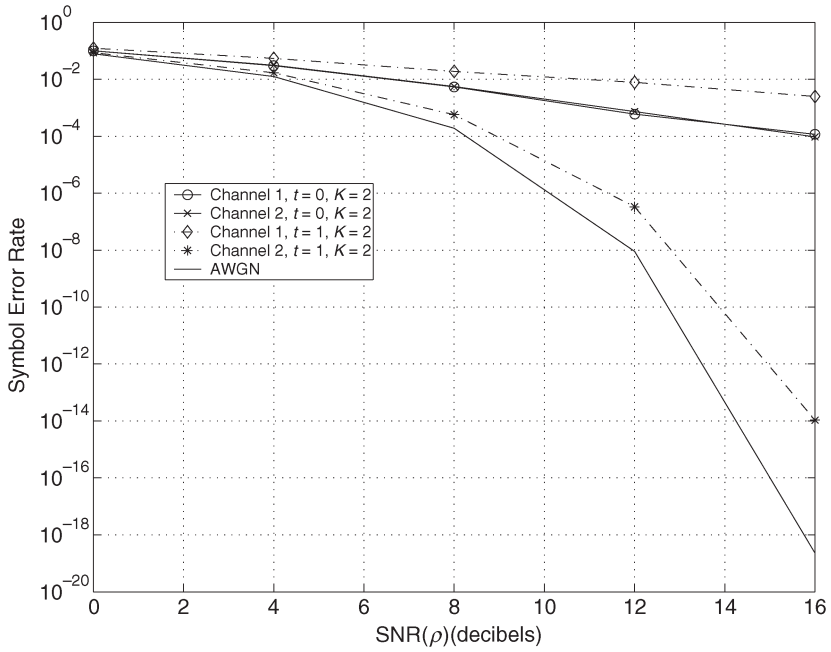

Fig. 4. Impact of the Hermitian angle between $\overline{\mathbf{h}}$ and $\mathcal{R}(\mathbf{R})$ on average uncoded symbol error rate performance. Both channels perform equally well when $t = 0$, but show drastically different behavior for $t = 1$.

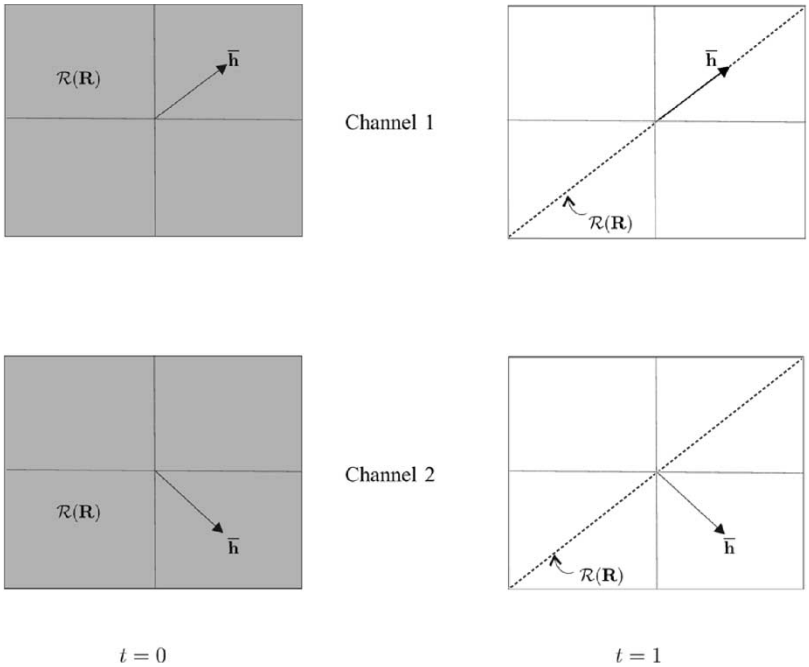

Fig. 5. Simplified graphical interpretation of Numerical Example 1 (for ease of visualization, we take $\mathcal{R}(\mathbf{R})$ to be two-dimensional).

well as the eigenvalue spread of $\mathbf{R}$ no longer have an impact on average error rate performance.

A. Numerical Example 2

This example demonstrates the critical impact of the Hermitian angle $\angle(\overline{\mathbf{h}}, \mathcal{R}(\mathbf{R}))$ on uncoded average symbol error rate performance. We consider a system with $M_{\mathrm{T}} = 2$ and $M_{\mathrm{R}} = 1$ employing the Alamouti scheme ($r_c = 1$) and two different channels $\mathbf{H}_1$ and $\mathbf{H}_2$ having different fixed components $\overline{\mathbf{H}}_1 = [1 \;\; 1]$ and $\overline{\mathbf{H}}_2 = [1 \;\; -1]$, respectively, but the same fading components. Fig. 4 shows the empirically (through Monte Carlo simulation) calculated average symbol error rate for both channels for $K = 2$ and for transmit correlation coefficients of $t = 0$ and $t = 1$. The symbol error rate for an AWGN channel with $\|\mathbf{H}\|_F^2 = 2$ is plotted for comparison. For $t = 0$, we have $\mathbf{R} = (2/3)\mathbf{I}_2$ and, hence, $\angle(\overline{\mathbf{h}}_1, \mathcal{R}(\mathbf{R})) = \angle(\overline{\mathbf{h}}_2, \mathcal{R}(\mathbf{R})) = 0$ so that for both channels $d_{\mathrm{E}} = 2$. However, for $t = 1$, the performance of the two channels is completely different. For Channel 1, $\angle(\overline{\mathbf{h}}_1, \mathcal{R}(\mathbf{R})) = 0$ (see Fig. 5) and $d_{\mathrm{E}} = 1$, reflected by the slope of the average error rate curve at high SNR. For channel 2, we have $\angle(\overline{\mathbf{h}}_2, \mathcal{R}(\mathbf{R})) = \pi/2$ (see

Fig. 5) so that $d_{\mathrm{E}} = \infty$, reflected by the close proximity of the error rate curve to that for the AWGN channel. In the low-SNR regime, all channels perform identically as expected from (15).

VI. Packet Error Rate Performance

In this section, we study the impact of propagation conditions on PER as defined in Section III. More specifically, employing the power series expansion in (24), we compute the outage related diversity order $d_{\mathrm{O}}(R)$, defined in (6) as a function of the propagation parameters, and show that the conclusions obtained through an analysis of d_{E} are equivalent to those obtained from $d_{\mathrm{O}}(R)$. Consequently, we find an interesting relation between the notion of diversity order obtained from the average error probability for finite code books and diversity order obtained from PER assuming Gaussian code books. Moreover, the analysis presented in this section establishes the existence of a critical rate R_{crit}, below which Ricean fading channels behave like AWGN channels, in the sense that signaling with zero outage is possible. For rates above R_{crit}, the Ricean channel behaves like a Rayleigh fading channel. Interestingly, it can be shown that R_{crit} is a simple function of $\angle(\overline{\mathbf{h}}, \mathcal{R}(\mathbf{R}))$.

Our analysis is for the high-SNR case (i.e., $\rho \gg 1$), which allows us to approximate the cdf of $\|\mathbf{H}\|_F^2$ by retaining the first term in the power series expansion (24)

$$P_{\mathrm{out}}(R) \approx \left(\prod_{j=1}^{r(\mathbf{R})} \frac{1}{\sigma_j}\right) \left(\mathrm{e}^{-\sum_{j=1}^{r(\mathbf{R})} \frac{|b_j|^2}{\sigma_j^2}}\right) \times \frac{\left(\frac{\left(2^{\frac{R}{r_c}}-1\right) M_{\mathrm{T}}}{\rho} - \delta\right)^{r(\mathbf{R})}}{r(\mathbf{R})!} \; u\left(\frac{\left(2^{\frac{R}{r_c}}-1\right) M_{\mathrm{T}}}{\rho} - \delta\right) \quad (16)$$

where δ was defined in (12). We shall next distinguish the cases $\delta = 0$ and $\delta > 0$.

For $\delta = 0$, the unit-step function in (16) will be equal to 1 for all rates R so that

$$\log P_{\mathrm{out}}(R) = -\sum_{j=1}^{r(\mathbf{R})} \log \sigma_j - \sum_{j=1}^{r(\mathbf{R})} \frac{|b_j|^2}{\sigma_j^2} + r(\mathbf{R}) \log\left(\left(2^{\frac{R}{r_c}}-1\right) M_{\mathrm{T}}\right) - r(\mathbf{R}) \log \rho - \log(r(\mathbf{R})!).$$

Invoking (6), we find that for a fixed (SNR-independent) transmission rate R

$$d_{\mathrm{O}}(R) = r(\mathbf{R})$$

which is consistent with the finite code book result in (13). Note, however, that if the transmission rate grows as a function of SNR so that $R(\rho) = r_c \log(1 + (Z\rho/M_{\mathrm{T}}))$, where Z is an arbitrary positive constant, then $P_{\mathrm{out}}(R) = F(Z)$ for any SNR and, hence, $d_{\mathrm{O}}(R) = 0$, conforming with [31].

Let us proceed with the case $\delta > 0$. Investigating the argument of the unit-step function in (16), we obtain $P_{\mathrm{out}}(R)$ (see the equation at the bottom of the page), where $R_{\mathrm{crit}} = r_c \log(1 + (\delta\rho/M_{\mathrm{T}}))$ and may be interpreted as the rate supported by the projection of $\overline{\mathbf{h}}$ onto $\mathcal{N}(\mathbf{R})$. This result points to an interesting behavior. At transmission rates $R < R_{\mathrm{crit}}$, signaling with zero outage is possible, and the Ricean channel behaves like an AWGN channel. Consequently, we obtain $d_{\mathrm{O}}(R) = \infty$ in this case. Interestingly, up to the pre-log r_c, the critical rate R_{crit} is the capacity of an SISO AWGN channel with $\mathrm{SNR} = \delta\rho/M_{\mathrm{T}}$. Equivalently, we can say that the gain of the effective SISO AWGN channel is given by the length of the projection of $\overline{\mathbf{h}}$ onto the null space of $\mathbf{R}$ (see Fig. 3). Note that while (17), shown at the bottom of the page, presents the outage probability for high SNR, it follows from (24) or (25) (cf. the argument of the unit-step function) that the presence of a critical rate can be established at any SNR and without invoking any approximation for $P_{\mathrm{out}}(R)$. Finally, if the transmission rate is allowed to grow with SNR so that $R(\rho) = r_c \log(1 + (Z\rho/M_{\mathrm{T}}))$ with $Z \geq \delta$, then $d_{\mathrm{O}}(R) = 0$. If on the other hand, the transmission rate grows with SNR so that $R(\rho) = r_c \log(1 + (Z\rho/M_{\mathrm{T}}))$ with $Z < \delta$, then we are assured zero outage and once again we have $d_{\mathrm{O}}(R) = \infty$.

We can now summarize our findings by noting that for fixed (SNR-independent) transmission rate R

$$d_{\mathrm{O}}(R) = \begin{cases} \infty, & \delta > 0 \\ r(\mathbf{R}), & \delta = 0 \end{cases} \quad (18)$$

which is fully consistent with the behavior of d_{E} [cf. (13)] and confirms a similar equivalence made for average and outage error rates in the finite code book case [14]. Furthermore, we note that $R_{\mathrm{crit}} = 0$ if $\angle(\overline{\mathbf{h}}, \mathcal{R}(\mathbf{R})) = 0$ and $R_{\mathrm{crit}} > 0$ if $0 < \angle(\overline{\mathbf{h}}, \mathcal{R}(\mathbf{R})) \leq \pi/2$. Consequently, $R_{\mathrm{crit}} = 0$ for an SISO fading channel (unless $K = \infty$). Finally, we note that for $\delta = 0$ and arbitrary R, or for $\delta > 0$ with $R > R_{\mathrm{crit}}$, fixed $r(\mathbf{R})$, and small $|b_j|$ $(j = 1, 2, \ldots, N)$ (i.e., small K-factor), the spread of the σ_j determines the offset of the PER with minimum PER obtained if $\mathbf{R} = \xi \mathbf{I}_N$. This result is consistent with our findings for $\overline{P}_e$ in Section V.

A. Numerical Example 3

This example serves to demonstrate the impact of $\angle(\overline{\mathbf{h}}, \mathcal{R}(\mathbf{R}))$ on R_{crit} and outage performance. For $K = 2$,

$$P_{\mathrm{out}}(R) \begin{cases} = 0, & R < R_{\mathrm{crit}} \\ \approx \left(\prod_{j=1}^{r(\mathbf{R})} \frac{1}{\sigma_j}\right) \left(\mathrm{e}^{-\sum_{j=1}^{r(\mathbf{R})} \frac{|b_j|^2}{\sigma_j^2}}\right) \frac{\left(\frac{\left(2^{\frac{R}{r_c}}-1\right) M_{\mathrm{T}}}{\rho} - \delta\right)^{r(\mathbf{R})}}{r(\mathbf{R})!}, & R \geq R_{\mathrm{crit}} \end{cases} \quad (17)$$

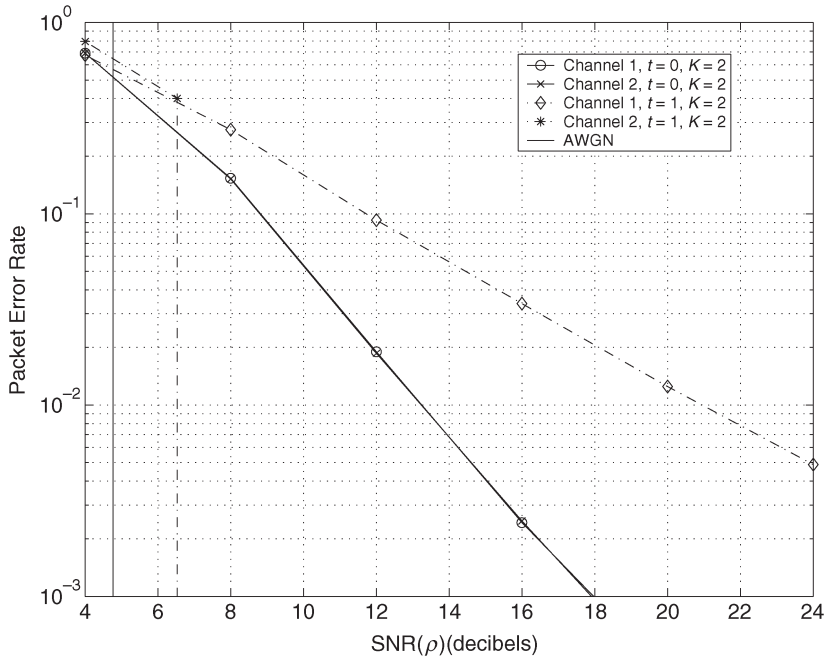

Fig. 6. Impact of the Hermitian angle between $\overline{\mathbf{h}}$ and $\mathcal{R}(\mathbf{R})$ on PER performance. Both channels perform equally well under independent fading (i.e., $t = 0$). For $t = 1$, channel 2 behaves like an AWGN channel for SNRs above 6.53 dB.

$R = 2$ bps/Hz and $\overline{\mathbf{H}}_1$ and $\overline{\mathbf{H}}_2$ defined in Numerical Example 2, Fig. 6 shows the empirically (through Monte Carlo simulation) calculated PER for the two channels for $t = 0$ and $t = 1$. In the uncorrelated case $t = 0$, $\delta = 0$, and, consequently, $R_{\text{crit}} = 0$ for both channels. Fig. 6 indeed shows that the two channels yield equal performance and exhibit Rayleigh fading behavior with $d_{\text{O}} = 2$ as suggested by (18). In the fully correlated case $t = 1$, $R_{\text{crit}} = 0$ for channel 1, which, combined with $r(\mathbf{R}) = 1$, yields a Rayleigh fading behavior as seen in Fig. 6. Channel 2, however, has a nonzero critical rate for $t = 1$ given by $R_{\text{crit}} = \log(1 + (2\rho/3))$ and, hence, behaves like an AWGN channel for SNRs above 6.53 dB. (The performance of an AWGN channel with $\|\mathbf{H}\|_F^2 = 2$ is shown for comparison.)

VII. Wideband Spectral Efficiency of OSTBCs

From our discussion in Section III, it is clear that under a total channel power constraint (i.e., $\|\mathbf{H}\|_F^2 + \mathcal{E}\{\|\widetilde{\mathbf{H}}\|_F^2\} \leq N$), the exact statistics of $\mathbf{H}$ do not have an impact on the minimum SNR per information bit required to sustain reliable communication, confirming the observation made previously in [9]. However, as will be seen in the following, the statistics of $\mathbf{H}$ do have a profound impact on the slope of wideband spectral efficiency as defined in [9]. Using (8), it is shown in the Appendix that

$$\mathcal{S} = 2r_c\left(\left(\frac{\text{Tr}(\mathbf{\Sigma}^2) + 2\overline{\mathbf{h}}^{\text{H}}\mathbf{R}\overline{\mathbf{h}}}{\left(\text{Tr}(\mathbf{\Sigma}) + \overline{\mathbf{h}}^{\text{H}}\overline{\mathbf{h}}\right)^2}\right) + 1\right)^{-1}. \qquad (19)$$

It is easily verified that (19) is equivalent to [22, eq. (18)] for the special case of MISO channels with $r_c = 1$, a consequence of the fact that OSTBCs are capacity optimal in such a scenario.

A. Pure Rayleigh Fading

Constraining the total average power in the channel to $\text{Tr}(\mathbf{\Sigma}) = N$, it is straightforward to show that $\mathcal{S}$ is maximized (or, equivalently, $\text{Tr}(\mathbf{\Sigma}^2)$ is minimized) when $\sigma_j = 1 (j = 1, 2, \ldots, N)$. This condition corresponds to i.i.d. fading, in which case $\mathcal{S} = 2r_c N/(N+1)$. We can see that in the infinite diversity limit $N \to \infty$, the wideband slope of the Rayleigh fading channel approaches the wideband slope of the AWGN channel (up to the factor r_c). Correlation matrix eigenvalue spread resulting from fading correlation and/or gain imbalance between channel elements will therefore reduce the wideband slope $\mathcal{S}$ through the term $\text{Tr}(\mathbf{\Sigma}^2)$, which is directly related to the "correlation number" defined in [22].

B. Ricean Fading

In the presence of Ricean fading, the wideband slope depends on the eigenvalue spread of $\mathbf{R}$ through the term $\text{Tr}(\mathbf{\Sigma}^2)$ and through the quadratic form $\overline{\mathbf{h}}^{\text{H}}\mathbf{R}\overline{\mathbf{h}}$. The Hermitian angle between $\overline{\mathbf{h}}$ and $\mathcal{R}(\mathbf{R})$ will impact the quadratic form $\overline{\mathbf{h}}^{\text{H}}\mathbf{R}\overline{\mathbf{h}}$; however, the delineation in performance is not as sharp as for the case of average or outage error rates. For example, $\overline{\mathbf{h}}^{\text{H}}\mathbf{R}\overline{\mathbf{h}}$ is minimum (i.e., 0) and, hence, the wideband slope is maximum (but finite) when $\angle(\overline{\mathbf{h}}, \mathcal{R}(\mathbf{R})) = \pi/2$. For $0 \leq \angle(\overline{\mathbf{h}}, \mathcal{R}(\mathbf{R})) < \pi/2$, the exact value of the wideband slope will depend on the geometry of $\overline{\mathbf{h}}$ relative to the geometry of the eigenvectors of $\mathbf{R}$. Unlike the cases of symbol error rate and PER, the wideband slope does not exhibit fundamentally different behavior in the cases of Rayleigh and Ricean fading. In both

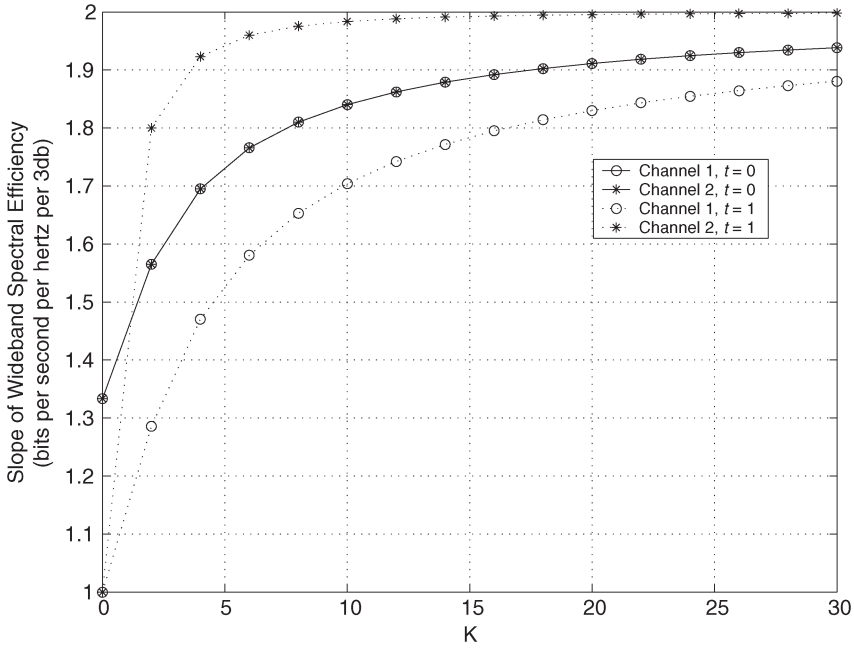

Fig. 7. Impact of the Hermitian angle between $\overline{\mathbf{h}}$ and $\mathcal{R}(\mathbf{R})$ on the slope of wideband spectral efficiency.

cases, the AWGN wideband slope of $\mathcal{S} = 2r_c$ can be achieved. As already mentioned in Section III, the wideband slope essentially measures the peakiness of the pdf of $\|\mathbf{H}\|_F^2$. The presence of a Ricean component results in faster convergence to the AWGN wideband slope.

C. Numerical Example 4

Following the setup in Numerical Examples 2 and 3, Fig. 7 plots $\mathcal{S}$ for the Alamouti scheme (i.e., $r_c = 1$) as a function of the K-factor. As expected, both channels exhibit the same performance for $t = 0$. In the correlated case $t = 1$, channel 2 outperforms channel 1, in the sense that convergence to the AWGN wideband slope is much faster. Furthermore, for $K = 0$, we can see that spatial fading correlation results in reduced $\mathcal{S}$ when compared to the uncorrelated case $t = 0$.

VIII. Conclusion

We characterized the impact of real-world propagation conditions on the maximum achievable diversity performance of communication over Ricean multiple-input multiple-output (MIMO) channels. Our analysis identified the Hermitian angle $\angle(\overline{\mathbf{h}}, \mathcal{R}(\mathbf{R}))$ and the eigenvalue spread of $\mathbf{R}$ as key quantities governing performance, irrespectively of the performance criterion used. For Ricean channels, we established the existence of a critical rate R_{crit}, below which signaling with zero outage is possible and, hence, the fading channel behaves like an AWGN channel. For rates above R_{crit}, the Ricean channel behaves like a Rayleigh fading channel. For fading SISO channels, R_{crit} is always zero, whereas in the MIMO case, R_{crit} is a simple function of $\angle(\overline{\mathbf{h}}, \mathcal{R}(\mathbf{R}))$. Finally, we showed that the notions of diversity order related to the slope of the average error probability versus SNR curve, and diversity order related to the slope of the outage probability versus SNR curve, yield equivalent results.

Appendix

MGF of $\|\mathbf{H}\|_F^2$

For a given $N \times 1$ vector $\mathbf{h} = \text{vec}(\mathbf{H})$, we start by defining the $2N \times 1$ vector $\mathbf{p} = [\Re(\mathbf{h})^{\text{T}}\ \Im(\mathbf{h})^{\text{T}}]^{\text{T}} = \overline{\mathbf{p}} + \widetilde{\mathbf{p}}$ with $\overline{\mathbf{p}} = [\Re(\overline{\mathbf{h}})^{\text{T}}\ \Im(\overline{\mathbf{h}})^{\text{T}}]^{\text{T}}$ and $\widetilde{\mathbf{p}} = [\Re(\widetilde{\mathbf{h}})^{\text{T}}\ \Im(\widetilde{\mathbf{h}})^{\text{T}}]^{\text{T}}$. The joint distribution of the elements of $\mathbf{p}$ is completely specified by the mean vector $\overline{\mathbf{p}} = \mathcal{E}\{\mathbf{p}\}$ and the $2N \times 2N$ covariance matrix $\mathbf{R}_p = \mathcal{E}\{\widetilde{\mathbf{p}}\widetilde{\mathbf{p}}^{\text{T}}\}$. Next, we establish a relation between the eigendecompositions of $\mathbf{R}$ and $\mathbf{R}_p$. For $\mathbf{R} = \mathbf{U}\mathbf{\Sigma}\mathbf{U}^{\text{H}}$ where $\mathbf{\Sigma} = \text{diag}\{\sigma_j\}_{j=1}^{N}$ (recall that $\sigma_j \geq \sigma_{j+1}$ for $j = 1, 2, \ldots, N-1$) and $\mathbf{R}_p = \mathbf{U}_p\mathbf{\Lambda}\mathbf{U}_p^{\text{T}}$, where $\mathbf{\Lambda} = \text{diag}\{\lambda_j\}_{j=1}^{2N}$, it is straightforward to show that

$$\mathbf{\Lambda} = \frac{1}{2}\begin{bmatrix} \mathbf{\Sigma} & \mathbf{0} \\ \mathbf{0} & \mathbf{\Sigma} \end{bmatrix} \quad \mathbf{U}_p = \begin{bmatrix} \Re(\mathbf{U}) & -\Im(\mathbf{U}) \\ \Im(\mathbf{U}) & \Re(\mathbf{U}) \end{bmatrix}.$$

Using the reduced eigendecomposition $\mathbf{R}_p = \widehat{\mathbf{U}}_p\widehat{\mathbf{\Lambda}}\widehat{\mathbf{U}}_p^{\text{T}}$ where $\widehat{\mathbf{\Lambda}} = \text{diag}\{\widehat{\lambda}_j\}_{j=1}^{2r(\mathbf{R})}$ with $\widehat{\lambda}_j (j = 1, 2, \ldots, 2r(\mathbf{R}))$ denoting the nonzero eigenvalues of $\mathbf{R}_p$, the MGF of $\mathbf{p}^{\text{T}}\mathbf{p} - (\overline{\mathbf{p}}^{\text{T}}\overline{\mathbf{p}} - \sum_{j=1}^{2r(\mathbf{R})}(r_j^2/\widehat{\lambda}_j))$ and the associated region of convergence (ROC) are obtained from [33] as

$$\begin{aligned}\widehat{\psi}(s) &= \mathcal{E}\left\{\text{e}^{-s\left(\mathbf{p}^{\text{T}}\mathbf{p} - \left(\overline{\mathbf{p}}^{\text{T}}\overline{\mathbf{p}} - \sum_{j=1}^{2r(\mathbf{R})}\frac{r_j^2}{\widehat{\lambda}_j}\right)\right)}\right\} \\ &= \exp\left\{-\sum_{j=1}^{2r(\mathbf{R})}\frac{r_j^2}{2\widehat{\lambda}_j^2} + 2\sum_{j=1}^{2r(\mathbf{R})}\frac{r_j^2}{(2\widehat{\lambda}_j)^3} \right. \\ &\qquad \left. \times\ s^{-1}\left(1 + \frac{1}{s2\widehat{\lambda}_j}\right)^{-1}\right\}\prod_{j=1}^{2r(\mathbf{R})}(1 + s2\widehat{\lambda}_j)^{-\frac{1}{2}}, \\ \text{ROC} &: \Re(s) > \max_{\widehat{\lambda}_j}\left(-\frac{1}{2\widehat{\lambda}_j}\right) \end{aligned} \tag{20}$$

where $r_j (j = 1, 2, \ldots, 2r(\mathbf{R}))$ denotes the jth element of $\mathbf{r} = \widehat{\mathbf{\Lambda}}^{1/2} \widehat{\mathbf{U}}_p^{\mathrm{T}} \overline{\mathbf{p}}$. Defining

$$\mathbf{b} = [\, b_1 \quad b_2 \quad \cdots \quad b_N \,]^{\mathrm{T}} = \mathbf{\Sigma}^{\frac{1}{2}} \mathbf{U}^{\mathrm{H}} \overline{\mathbf{h}}$$

it is easily seen that $\mathbf{r} = (1/\sqrt{2}) [\Re(\widehat{\mathbf{b}})^{\mathrm{T}} \; \Im(\widehat{\mathbf{b}})^{\mathrm{T}}]^{\mathrm{T}}$, where $\widehat{\mathbf{b}} = [b_1 \; b_2 \; \cdots \; b_{r(\mathbf{R})}]^{\mathrm{T}}$. Hence, $\mathbf{p}^{\mathrm{T}} \mathbf{p} - (\overline{\mathbf{p}}^{\mathrm{T}} \overline{\mathbf{p}} - \sum_{j=1}^{2r(\mathbf{R})} (r_j^2 / \widehat{\lambda}_j)) = \|\mathbf{H}\|_F^2 - (\|\overline{\mathbf{H}}\|_F^2 - \sum_{j=1}^{r(\mathbf{R})} (|b_j|^2 / \sigma_j))$ so that (20) can be written as

$$\widehat{\psi}(s) = \prod_{j=1}^{r(\mathbf{R})} (1 + s\sigma_j)^{-1} \times \exp\left\{ - \sum_{j=1}^{r(\mathbf{R})} \frac{|b_j|^2}{\sigma_j^2} + \sum_{j=1}^{r(\mathbf{R})} \frac{|b_j|^2}{\sigma_j^3} s^{-1} \left(1 + \frac{1}{s\sigma_j}\right)^{-1} \right\}$$

$$\mathrm{ROC} : \Re(s) > \max_{\sigma_j} \left(-\frac{1}{\sigma_j} \right). \tag{21}$$

Summarizing our results, we obtain the MGF of $\|\mathbf{H}\|_F^2$ as

$$\psi(s) = \mathcal{E}\left\{ \mathrm{e}^{-s\|\mathbf{H}\|_F^2} \right\} = \exp\left\{ -s \left(\|\overline{\mathbf{H}}\|_F^2 - \sum_{j=1}^{r(\mathbf{R})} \frac{|b_j|^2}{\sigma_j} \right) \right\} \widehat{\psi}(s). \tag{22}$$

Power Series Expansion for the cdf of $\|\mathbf{H}\|_F^2$

Following the series expansion approach in [33] with appropriate modifications to reflect the complex Gaussian nature of the elements of $\mathbf{H}$, we shall next use (21) to derive a power series expansion for the cdf of $\|\mathbf{H}\|_F^2$. Defining

$$M(\theta) = \left(\prod_{j=1}^{r(\mathbf{R})} \frac{1}{\sigma_j} \right) \left(\prod_{j=1}^{r(\mathbf{R})} \left(1 + \frac{\theta}{\sigma_j}\right)^{-1} \right) \times \exp\left\{ \sum_{j=1}^{r(\mathbf{R})} \frac{|b_j|^2 \theta}{\sigma_j^3} \left(1 + \frac{\theta}{\sigma_j}\right)^{-1} - \sum_{j=1}^{r(\mathbf{R})} \frac{|b_j|^2}{\sigma_j^2} \right\}$$

we can write (21) as

$$\widehat{\psi}(s) = s^{-r(\mathbf{R})} M\left(\frac{1}{s}\right). \tag{23}$$

In [33], it is shown that $M(\theta)$ can be expressed as a power series of the form $M(\theta) = \sum_{k=0}^{\infty} c_k \theta^k$ with

$$c_0 = \left(\prod_{j=1}^{r(\mathbf{R})} \frac{1}{\sigma_j} \right) \exp\left(- \sum_{j=1}^{r(\mathbf{R})} \frac{|b_j|^2}{\sigma_j^2} \right)$$

$$c_k = \frac{1}{k} \sum_{r=0}^{k-1} d_{k-r} c_r \quad \text{for} \quad k \geq 1$$

where $d_0 = -\sum_{j=1}^{r(\mathbf{R})} \ln(\sigma_j) - \sum_{j=1}^{r(\mathbf{R})} (|b_j|^2 / \sigma_j^2)$ and $d_k = (-1)^k \sum_{j=1}^{r(\mathbf{R})} ((1/\sigma_j^k) - (k|b_j|^2 / \sigma_j^{k+2}))$ for $k \geq 1$. Using (23), it follows that[3]

$$\widehat{\psi}(s) = \sum_{k=0}^{\infty} c_k s^{-(r(\mathbf{R})+k)}$$

which lends itself readily to Laplace transform inversion followed by integration to give the cdf of $\|\mathbf{H}\|_F^2$ as

$$F(y) = \sum_{k=0}^{\infty} c_k \frac{(y-\delta)^{r(\mathbf{R})+k}}{(r(\mathbf{R})+k)!} u(y-\delta) \tag{24}$$

where $\delta = \|\overline{\mathbf{H}}\|_F^2 - \sum_{j=1}^{r(\mathbf{R})} (|b_j|^2 / \sigma_j)$.

Laguerre Series Expansion for the cdf of $\|\mathbf{H}\|_F^2$

As for the power series expansion, the Laguerre series expansion approach in [33] can be adapted to the complex-valued case with appropriate modifications. For the sake of conciseness, we state the result without derivation

$$F(y) = \left(1 - \sum_{i=0}^{r(\mathbf{R})-1} \frac{\left(\frac{y-\delta}{2\beta}\right)^{r(\mathbf{R})-1-i}}{(r(\mathbf{R})-1-i)!} \, \mathrm{e}^{-\frac{y-\delta}{2\beta}} \right) u(y-\delta) + \left(\sum_{k=1}^{\infty} \widetilde{c}_k \frac{(k-1)!}{(r(\mathbf{R})+k-1)!} \left(\frac{y-\delta}{2\beta}\right)^{r(\mathbf{R})} \times \mathrm{e}^{-\frac{y-\delta}{2\beta}} \boldsymbol{L}_{k-1}^{(r(\mathbf{R}))} \left(\frac{y-\delta}{2\beta}\right) \right) u(y-\delta) \tag{25}$$

where β is an arbitrary positive constant whose role will be made clear shortly and $\boldsymbol{L}_k^{(\alpha)}(x)$ $(\alpha > -1, k = 0, 1, \ldots)$ denotes the generalized Laguerre polynomial given by

$$\boldsymbol{L}_k^{(\alpha)}(x) = \sum_{r=0}^{k} \left(\frac{(-x)^r}{r!(k-r)!} \prod_{n=r+1}^{k} (\alpha + n) \right)$$

and the coefficients $\widetilde{c}_k (k \geq 1)$ can be calculated recursively through the relation

$$\widetilde{c}_k = \frac{1}{k} \sum_{r=0}^{k-1} \widetilde{d}_{k-r} \widetilde{c}_r$$

where $\widetilde{c}_0 = 1$ and

$$\widetilde{d}_k = -\frac{k}{2\beta} \sum_{j=1}^{r(\mathbf{R})} \frac{|b_j|^2}{\sigma_j} \left(1 - \frac{\sigma_j}{2\beta}\right)^{k-1} + \sum_{j=1}^{r(\mathbf{R})} \left(1 - \frac{\sigma_j}{2\beta}\right)^k, \quad k \geq 1.$$

[3]We note that d_k as specified in [33, eq. 4.2b.10] for the real-valued case is incorrect as the factor $(-1)^k$ is missing.

The convergence properties of the series expansion in (25) depend strongly on the choice of β. We observed that choosing β to satisfy $1 \leq \beta \leq 4$ typically results in fast convergence.

Standard Deviation of $\|\mathbf{H}\|_F^2$

We start by noting that $\|\mathbf{H}\|_F^2 = \overline{\mathbf{h}}^{\mathrm{H}}\overline{\mathbf{h}} + \widetilde{\mathbf{h}}^{\mathrm{H}}\widetilde{\mathbf{h}} + 2\Re(\overline{\mathbf{h}}^{\mathrm{H}}\widetilde{\mathbf{h}})$. Using $2\Re(\overline{\mathbf{h}}^{\mathrm{H}}\widetilde{\mathbf{h}}) \sim \mathcal{N}(0, 2\overline{\mathbf{h}}^{\mathrm{H}}\mathbf{R}\overline{\mathbf{h}})$, it is easy to show that the random variables $\widetilde{\mathbf{h}}^{\mathrm{H}}\widetilde{\mathbf{h}}$ and $2\Re(\overline{\mathbf{h}}^{\mathrm{H}}\widetilde{\mathbf{h}})$ are uncorrelated. Consequently, $\sigma^2 = \mathrm{var}(\|\mathbf{H}\|_F^2) = \mathrm{var}(\widetilde{\mathbf{h}}^{\mathrm{H}}\widetilde{\mathbf{h}}) + \mathrm{var}(2\Re(\overline{\mathbf{h}}^{\mathrm{H}}\widetilde{\mathbf{h}}))$. Noting that $\widetilde{\mathbf{h}}^{\mathrm{H}}\widetilde{\mathbf{h}} = \widetilde{\mathbf{p}}^{\mathrm{T}}\widetilde{\mathbf{p}}$ and $\mathrm{var}(\widetilde{\mathbf{p}}^{\mathrm{T}}\widetilde{\mathbf{p}}) = 2\mathrm{Tr}(\mathbf{R}_p^2) = \mathrm{Tr}(\mathbf{\Sigma}^2)$, we finally obtain

$$\sigma = \sqrt{\mathrm{Tr}(\mathbf{\Sigma}^2) + 2\overline{\mathbf{h}}^{\mathrm{H}}\mathbf{R}\overline{\mathbf{h}}}.$$

ACKNOWLEDGMENT

The authors would like to thank the anonymous reviewers and the associate editor for their useful comments on the paper.

REFERENCES

[1] J. Guey, M. P. Fitz, M. R. Bell, and W. Kuo, "Signal design for transmitter diversity wireless communication systems over Rayleigh fading channels," in *Proc. IEEE Vehicular Technology Conf. (VTC)*, Atlanta, GA, Apr./May 1996, vol. 1, pp. 136–140.

[2] V. Tarokh, N. Seshadri, and A. R. Calderbank, "Space–time codes for high data rate wireless communication: Performance criterion and code construction," *IEEE Trans. Inf. Theory*, vol. 44, no. 2, pp. 744–765, Mar. 1998.

[3] S. M. Alamouti, "A simple transmit diversity technique for wireless communications," *IEEE J. Sel. Areas Commun.*, vol. 16, no. 8, pp. 1451–1458, Oct. 1998.

[4] V. Tarokh, H. Jafarkhani, and A. R. Calderbank, "Space–time block codes from orthogonal designs," *IEEE Trans. Inf. Theory*, vol. 45, no. 5, pp. 1456–1467, Jul. 1999.

[5] D. S. Baum, D. Gore, R. Nabar, S. Panchanathan, K. V. S. Hari, V. Erceg, and A. J. Paulraj, "Measurement and characterization of broadband MIMO fixed wireless channels at 2.5 GHz," in *Proc. IEEE Int. Conf. Personal Wireless Communications (ICPWC)*, Hyderabad, India, Dec. 2000, pp. 203–206.

[6] A. Paulraj, R. Nabar, and D. Gore, *Introduction to Space–Time Wireless Communications*. Cambridge, U.K.: Cambridge Univ. Press, 2003.

[7] L. H. Ozarow, S. Shamai, and A. D. Wyner, "Information theoretic considerations for cellular mobile radio," *IEEE Trans. Veh. Technol.*, vol. 43, no. 2, pp. 359–378, May 1994.

[8] J. Proakis, *Digital Communications*, 3rd ed. New York: McGraw-Hill, 1995.

[9] S. Verdú, "Spectral efficiency in the wideband regime," *IEEE Trans. Inf. Theory*, vol. 48, no. 6, pp. 1319–1343, Jun. 2002.

[10] W. C. Jakes, *Microwave Mobile Communications*. New York: Wiley, 1974.

[11] M. K. Simon and M. S. Alouini, *Digital Communication Over Fading Channels: A Unified Approach to Performance Analysis*. New York: Wiley, 2000.

[12] Y. Ko, M. S. Alouini, and M. K. Simon, "Outage probability of diversity systems over generalized fading channels," *IEEE Trans. Commun.*, vol. 48, no. 11, pp. 1783–1787, Nov. 2000.

[13] M. S. Alouini, A. Abdi, and M. Kaveh, "Sum of gamma variates and performance of wireless communication systems over Nakagami-fading channels," *IEEE Trans. Veh. Technol.*, vol. 50, no. 6, pp. 1471–1480, Nov. 2001.

[14] Z. Wang and G. B. Giannakis, "A simple and general parameterization quantifying performance in fading channels," *IEEE Trans. Commun.*, vol. 51, no. 8, pp. 1389–1398, Aug. 2003.

[15] M. P. Fitz, J. Grimm, and S. Siwamogsatham, "A new view of performance analysis techniques in correlated Rayleigh fading," in *Proc. IEEE Wireless Communications and Networking Conf. (WCNC)*, New Orleans, LA, Sep. 1999, vol. 1, pp. 139–144.

[16] H. Bölcskei and A. J. Paulraj, "Performance analysis of space–time codes in correlated Rayleigh fading environments," in *Proc. Asilomar Conf. Signals, Systems and Computers*, Pacific Grove, CA, Nov. 2000, vol. 1, pp. 687–693.

[17] H. Bölcskei, M. Borgmann, and A. J. Paulraj, "Impact of the propagation environment on the performance of space–frequency coded MIMO-OFDM," *IEEE J. Sel. Areas Commun.*, vol. 21, no. 3, pp. 427–439, Apr. 2003.

[18] M. K. Simon, "A moment generating function (MGF)-based approach for performance evaluation of space–time coded communication systems," *Wiley J. Wireless Commun. Mobile Comput.*, vol. 2, no. 7, pp. 667–692, Nov. 2002.

[19] M. Uysal and C. N. Georghiades, "Effect of spatial fading correlation on performance of space–time codes," *Electron. Lett.*, vol. 37, no. 3, pp. 181–183, Feb. 2001.

[20] ——, "Upper bounds on the BER performance of MTCM-STBC schemes over shadowed Rician fading channels," in *Proc. IEEE Vehicular Technology Conf. (VTC Fall)*, Vancouver, BC, Canada, Sep. 2002, vol. 1, pp. 62–66.

[21] M. Gharavi-Alkhansari and A. B. Gershman, "Exact symbol error probability of space–time block codes," in *Proc. Asilomar Conf. Signals, Systems, and Computers*, Pacific Grove, CA, Nov. 2003, vol. 2, pp. 1835–1839.

[22] A. Lozano, A. M. Tulino, and S. Verdú, "Multiple-antenna capacity in the low-power regime," *IEEE Trans. Inf. Theory*, vol. 49, no. 10, pp. 2527–2544, Oct. 2003.

[23] E. Biglieri, J. Proakis, and S. Shamai, "Fading channels: Information-theoretic and communications aspects," *IEEE Trans. Inf. Theory*, vol. 44, no. 6, pp. 2619–2692, Oct. 1998.

[24] G. Stüber, *Principles of Mobile Communication*. Norwell, MA: Kluwer, 1996.

[25] D. Shiu, G. Foschini, M. Gans, and J. Kahn, "Fading correlation and its effect on the capacity of multi-element antenna systems," *IEEE Trans. Commun.*, vol. 48, no. 3, pp. 502–513, Mar. 2000.

[26] D. Gesbert, H. Bölcskei, D. A. Gore, and A. J. Paulraj, "Outdoor MIMO wireless channels: Models and performance prediction," *IEEE Trans. Commun.*, vol. 50, no. 12, pp. 1926–1934, Dec. 2002.

[27] J. M. Cioffi. (2003). *Class Reader for EE379a—Digital Communication: Signal Processing*. Stanford, CA: Stanford Univ. [Online]. Available: http://www.stanford.edu/class/ee379a

[28] S. Benedetto and E. Biglieri, *Principles of Digital Transmission With Wireless Applications*. Norwell, MA: Kluwer, 1999.

[29] J. Ventura-Traveset, G. Caire, E. Biglieri, and G. Taricco, "Impact of diversity reception on fading channels with coded modulation—Part I: Coherent detection," *IEEE Trans. Commun.*, vol. 45, no. 5, pp. 676–686, May 1997.

[30] T. M. Cover and J. A. Thomas, *Elements of Information Theory*. New York: Wiley, 1991.

[31] L. Zheng and D. N. C. Tse, "Diversity and multiplexing: A fundamental tradeoff in multiple-antenna channels," *IEEE Trans. Inf. Theory*, vol. 49, no. 5, pp. 1073–1096, May 2003.

[32] U. Charash, "A study of multipath reception with unknown delays," Ph.D. thesis, Dept. Elect. Eng., Univ. California, Berkeley, Jan. 1974.

[33] A. M. Mathai and S. B. Provost, *Quadratic Forms in Random Variables*. New York: Marcell Dekker, 1992.

[34] D. Raphaeli, "Distribution of noncentral quadratic forms in complex normal variables," *IEEE Trans. Inf. Theory*, vol. 42, no. 3, pp. 1002–1006, May 1996.

[35] M. O. Hasna, M. S. Alouini, and M. K. Simon, "Effect of fading correlation on the outage probability of cellular mobile radio systems," in *Proc. IEEE Vehicular Technology Conf. (VTC)*, Atlantic City, NJ, Oct. 2001, vol. 3, pp. 1794–1798.

[36] S. Kotz, N. L. Johnson, and D. W. Boyd, "Series representations of distributions of quadratic forms in normal random variables II: Non-central case," *Ann. Math. Stat.*, vol. 38, pp. 838–848, 1967.

[37] K. Scharnhorst, "Angles in complex vector spaces," *Acta Appl. Math.*, vol. 69, no. 1, pp. 95–103, Oct. 2001.

Rohit U. Nabar (S'02–M'03) was born in Bombay, India, on December 18, 1976. He received the B.S. degree (*summa cum laude*) in electrical engineering from Cornell University, Ithaca, NY, in 1998, and the M.S. and Ph.D. degrees in electrical engineering from Stanford University, Stanford, CA, in 2000 and 2003 respectively. His doctoral research focused on signaling for real-world multiple-input multiple-output (MIMO) channels.

From 2002 to 2004, he was a Postdoctoral Researcher in the Communication Theory Group, Swiss Federal Institute of Technology (ETH), Zurich, Switzerland. Between 2004–2005, he was a Faculty Member at the Communications and Signal Processing Research Group, Department of Electrical and Electronic Engineering, Imperial College, London, U.K. Since July 2005, he has been a member of the DSP Technology Group at Marvell Semiconductor, Inc., Sunnyvale, CA. His research interests include signal processing and information theory for wireless communications and networks. He has coauthored (with A. Paulraj and D. Gore) the textbook *Introduction to Space–Time Wireless Communications* (Cambridge, U.K.: Cambridge Univ. Press, 2003).

Dr. Nabar was a Member of the Smart Antennas Research Group at Stanford and a recipient of the Dr. T. J. Rodgers Stanford graduate fellowship. He currently serves as an Associate Editor for the IEEE COMMUNICATIONS LETTERS.

Helmut Bölcskei (M'98–SM'02) was born in Austria on May 29, 1970. He received the Dr.techn. degree in electrical engineering from the Vienna University of Technology, Vienna, Austria, in 1997.

In 1998, he was a Postdoctoral Researcher at Vienna University of Technology. From 1999 to 2001, he was a postdoctoral researcher in the Information Systems Laboratory, Department of Electrical Engineering, Stanford University, Stanford, CA. During that period, he was also a consultant for Iospan Wireless, Inc., Palo Alto, CA. From 2001 to 2002, he was an Assistant Professor of Electrical Engineering at the University of Illinois at Urbana-Champaign. Since 2002, he has been an Assistant Professor of Communication Theory at the Swiss Federal Institute of Technology (ETH) Zürich, Zürich, Switzerland. He was a Visiting Researcher at Philips Research Laboratories Eindhoven, The Netherlands, ENST Paris, France, and the Heinrich Hertz Institute Berlin, Germany. His research interests include communication and information theory with special emphasis on wireless communications and signal processing.

Dr. Bölcskei received a 2001 IEEE Signal Processing Society Young Author Best Paper Award and was an Erwin Schrödinger Fellow (1999–2001) of the Austrian National Science Foundation (FWF). He was an Associate Editor for the IEEE TRANSACTIONS ON SIGNAL PROCESSING and the *EURASIP Journal on Applied Signal Processing*, and is currently an Associate Editor for the IEEE TRANSACTIONS ON WIRELESS COMMUNICATIONS and serves on the editorial board of *Foundations and Trends in Networking*.

Arogyaswami J. Paulraj (SM'85–F'91) received the Ph.D. degree from the Naval Engineering College and the Indian Institute of Technology, New Delhi, India.

He is a Professor at the Department of Electrical Engineering, Stanford University, Stanford, CA, where he supervises the Smart Antennas Research Group, working on applications of space–time techniques for wireless communications. His nonacademic positions included Head, Sonar Division, Naval Oceanographic Laboratory, Cochin, India; Director, Center for Artificial Intelligence and Robotics, Bangalore, India; Director, Center for Development of Advanced Computing, Pune, India; Chief Scientist, Bharat Electronics, Bangalore, India; Chief Technical Officer and Founder, Iospan Wireless, Inc., Palo Alto, CA. His research has spanned several disciplines, emphasizing estimation theory, sensor signal processing, parallel computer architectures/algorithms and space–time wireless communications. His engineering experience has included development of sonar systems, massively parallel computers, and broadband wireless systems. He is the author of over 300 research publications and holds 8 patents.

Dr. Paulraj has won several awards for his engineering and research contributions, including the IEEE Signal Processing Society's Technical Achievement Award. He is a member of the Indian National Academy of Engineering.